

# Contact Engineering of Halide Perovskites: Gold is Not Good Enough; Metalloid is Better

Zhengxun Lai, Yuxuan Zhang, You Meng, Xiuming Bu, Wei Wang, Pengshan Xie, Weijun Wang, Chuntai Liu, SenPo Yip, and Johnny C. Ho\*

The operation stability of halide perovskite devices is the critical issue that impedes their commercialization. The main reasons are that the ambient H<sub>2</sub>O molecules can easily deteriorate the perovskites, while the metal electrodes react in different degrees with the perovskites. Herein, one kind of new electrode, the metalloids, is reported, which are much more stable than the conventional noble metals as electrical contacts for halide perovskites. The degradation mechanism of halide perovskites with noble metal electrodes is carefully studied and compared with the metalloid electrodes. It is found that the iodide ions can easily halogenate Cu and Ag in halide perovskites. Although Au is almost not halogenated, it can also decompose the perovskite film. On the contrary, after long-term storage, the metalloid electrodes remain intact on the perovskite film without any degradation. In addition, the long-time operation stability of the perovskite devices with metalloid electrodes is much higher than that of noble metals. First-principles calculations confirm the exceptional stability of the metalloid electrodes. This work explores the ultra-stable electrodes for halide perovskites, paving the way to the large-scale deployment of perovskite-based electronic devices.

promising candidates for next-generation solar cells, light-emitting diodes, photodetectors, phototransistors, etc.<sup>[1–4]</sup> Unfortunately, the stability of halide perovskites is rather poor, being the main obstacle to the deployment of these charming materials.<sup>[5–8]</sup> In fact, halide perovskite devices always degrade irreversibly at high temperatures, in humid environments, or by reacting with contact electrodes during the operation.<sup>[9,10]</sup> The temperature and humidity issues can be somewhat alleviated using appropriate packaging techniques.<sup>[11–13]</sup> However, the electrode problem still exists because almost all the metal electrodes would react with the halogens in halide perovskites.<sup>[14–18]</sup> Even the relatively inert metal electrodes, such as Cu and Ag, can easily deteriorate the material properties of halide perovskites when they are electrically contacted.<sup>[19,20]</sup> Normally, the noble

metal, particularly Au, is the first choice and the most used metal electrode for halide perovskite devices because of its exceptional chemical stability.<sup>[21,22]</sup> One drawback is that Au can actually diffuse into perovskite materials and react with the constituent.<sup>[23,24]</sup> Another issue is that Au is too expensive, which is not conducive for future large-scale applications. Recently, carbon electrodes have also been proposed as stable electrodes for halide perovskites.<sup>[25,26]</sup> Nevertheless, the limited deposition method of carbon electrodes makes them hardly be patterned for device fabrication, which greatly limits their practical utilization. More importantly, the device performance with carbon electrodes is far from satisfactory compared to noble metal electrodes-based halide perovskite devices.<sup>[27,28]</sup> In this regard, it is essential to thoroughly study the reaction mechanism between the frequently used contact electrodes (e.g., Au, Cu, and Ag) and the halide perovskites. Once a good understanding of contact engineering is obtained, the design and development of efficient, robust, and stable contact electrodes for halide perovskite devices can be achieved.

Apart from noble metals, metalloids are also suitable as electrode materials.<sup>[29]</sup> As shown in **Figure 1a**, metalloids are located in a jagged zone between the two regions of metals and nonmetals, which endows them with the characteristics of both metals and nonmetals. The metallic conducting behavior of metalloids makes them capable of playing the role of electrodes.

## 1. Introduction

Due to their excellent photoelectric properties and continuously tunable bandgap, halide perovskites are one of the most

Z. Lai, Y. Zhang, Y. Meng, X. Bu, W. Wang, P. Xie, W. Wang, J. C. Ho  
Department of Materials Science and Engineering  
City University of Hong Kong  
Kowloon, Hong Kong SAR 999077, China  
E-mail: johnnyho@cityu.edu.hk

Y. Meng, J. C. Ho  
State Key Laboratory of Terahertz and Millimeter Waves  
City University of Hong Kong  
Kowloon, Hong Kong SAR 999077, China

C. Liu  
Key Laboratory of Advanced Materials Processing & Mold (Zhengzhou University)  
Ministry of Education  
Zhengzhou 450002, China

S. Yip, J. C. Ho  
Institute for Materials Chemistry and Engineering  
Kyushu University  
Fukuoka 816–8580, Japan

 The ORCID identification number(s) for the author(s) of this article can be found under <https://doi.org/10.1002/smt.202201567>

DOI: 10.1002/smt.202201567

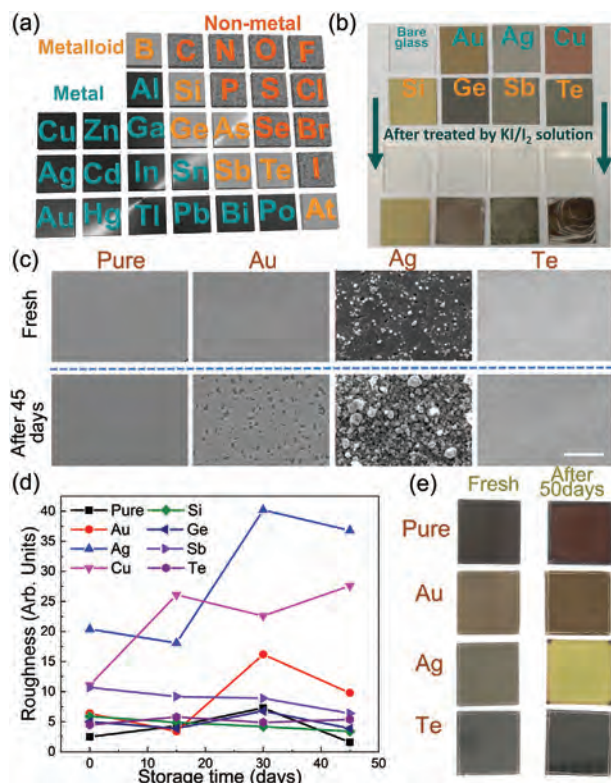


**Figure 1.** a) Metalloids in the periodic table. b) Before and after etching the metals and metalloids by the  $KI/I_2$  solution. c) Scanning electron microscope (SEM) images of the pure organic-inorganic halide perovskite (OIHP) film and the films with Au, Ag, and Te electrodes before and after the storage for 45 days, where they share the same scale bar of 2  $\mu m$ . d) Changes in the roughness of the OIHP films with different metal and metalloid electrodes during storage. e) Photographs of the pure OIHP film and the films with Au, Ag, and Te electrodes on glass substrates before and after storage for 50 days, where the side lengths of these glass slides are 15 mm.

At the same time, the nonmetallic character of metalloids also gives them high electronegativity, which makes them hardly corroded.<sup>[30]</sup> As a result, it is ideal to consider metalloids as one kind of superior material for the contact electrodes of halide perovskites. In this work, the metalloid electrodes, including Si, Ge, Sb, and Te, are systematically investigated in their reaction kinetics with halide perovskites and contrasted with the other typical noble metal counterparts (e.g., Au, Cu, and Ag). The other metalloids, such as B, As, and At are not examined because the melting point of B is too high for thermal deposition, As is highly toxic, and At is radioactive; hence, these “unfriendly” metalloids are not appropriate as contact electrodes. Impressively, using different characterization techniques, it is revealed that the “friendly” metalloids exhibit outstanding contact stability with halide perovskite devices even for long-duration operation, which is not achievable with the noble metal electrodes. The first-principles calculation further proves that the metalloid electrodes can not only stay stable as the electrodes but also protect the halide perovskite materials from being deteriorated by  $H_2O$ . All these findings have evidently tackled the contact electrode stability problem

of halide perovskites, paving the way to the large-scale deployment of perovskite-based electronic devices.

## 2. Results and Discussion

First of all, as we anticipate the metalloid electrodes are robust and stable for the perovskite device operation, it is important to evaluate their chemical stability. Actually, it is well known that noble metal electrodes can be easily oxidized by halide ions, particularly  $I^-$ , in halide perovskites. For instance, the  $KI/I_2$  solution, containing large amounts of  $I^-$  ions, is a common etching solution for Au and other noble metals, including Ag and Cu.<sup>[31–33]</sup> Here, the  $KI/I_2$  solution is then utilized as an etching solution to investigate the corrosion resistance of metalloids. The metal and metalloid films with a thickness of 50 nm were thermally evaporated on standard glass slides, while one bare glass slide was used as a control sample. It needs to be pointed out that the thickness of the films can be accurately controlled through the thickness monitor integrated with the deposition equipment. The thicknesses,  $t$ , of these films can also be verified by atomic force microscopy (AFM), as shown in Figure S1 (Supporting Information). As demonstrated in Figure 1b, after being immersed in the  $I_2/KI$  solution for 10 s, the noble metal films of Au, Ag, and Cu were completely etched away. On the contrary, most parts of the metalloid films of Si, Ge, Sb, and Te can remain intact after etching. Notably, one can see that the Si film can even keep unaffected by soaking in the  $KI/I_2$  solution. These results reveal that the halide ions can hardly corrode the metalloid materials, indicating the promising potential of using metalloid electrodes, instead of noble metal electrodes, for the prolonged and stable operation of halide perovskite devices.

After confirming the superior stability of metalloid materials with iodine ions, evaluating their electrode stability as electrical contacts to different halide perovskite devices is essential. To be specific, the typical noble metal electrodes of Au, Ag, and Cu and metalloid electrodes of Si, Ge, Sb, and Te were thermally evaporated on both OIHP and all-inorganic halide perovskite (AIHP) films fabricated by a spin-coating method. For OIHP, the quasi-2D halide perovskite of  $(iBA)_2(MA)_3Pb_4I_{13}$  ( $iBA = C_4H_9NH_3I$  and  $MA = CH_3NH_3I$ ) was employed due to its superior stability as compared to its 3D counterpart of  $MAPbI_3$ . The high-intensity and typical X-ray diffraction (XRD) peaks of this quasi-2D halide perovskite can also help to understand the influence of electrodes in subsequent studies. For AIHP,  $CsPbBr_3$  was chosen because of its excellent phase stability. This good stability of the OIHP and AIHP materials we chose would eliminate the influence of their self-decay on our experiment. All these perovskite films deposited with 50-nm-thick metals or metalloids were next stored in a glove box, where the  $O_2$  and  $H_2O$  concentrations are well-controlled to less than 1 ppm to prevent the decomposition of the films. One pristine perovskite film without any electrode was also stored and studied as a control sample. As depicted in the SEM images in Figure 1c and Figures S2 and S3 (Supporting Information), it is observed that for Ag and Cu samples, there are holes and nucleation on the fresh films suggesting Ag and Cu could directly react with the OIHP films once they were deposited. After being stored in the glove box for 15, 30, and 45 days, the Ag and Cu samples decayed gradually. Even for the Au sample, there were apparent pinholes, and the films became rougher

after 30 and 45 days. On the other hand, for the metalloid samples and pure OIHPs, the films stayed smooth and intact after storage, illustrating metalloids can serve as more stable electrodes for OIHPs than noble metals. The SEM images of the pure metal and metalloid films deposited on bare glass slides are also shown in Figure S4 (Supporting Information) as a control. One can see all the films are smooth, and the grains of the Sb film are obvious due to the large sizes. The change in the samples' roughness was then characterized using the ImageJ software and displayed in Figure 1d. The roughness of the Ag and Cu samples is much larger than the others and increases with the storage time. The Au sample also decayed and became rougher as the storage time grew. However, the metalloid samples (i.e., Si, Ge, and Te) stay with the same roughness as the pure OIHP film, which does not change after storage. It needs to be pointed out that the roughness of the Sb sample is a little larger due to its large grains just mentioned, but the surface morphology can still maintain the same after 45 days. All these results indicate the metalloids can barely react with the OIHPs, which performed much better than the noble metals, even Au. The SEM images of the AIHP films with different metal and metalloid electrodes are as well shown in Figures S5 and S6 (Supporting Information). There are typical gullies on the spin-coated CsPbBr<sub>3</sub> films due to their poor solubility in the precursor solution, which has been reported before.<sup>[34,35]</sup> Nevertheless, these gullies could enlarge the contact area between the CsPbBr<sub>3</sub> films and the electrodes, which was beneficial for us to study their reaction. After 15 days, obvious coatings appeared on the Ag, Cu, and even Au samples, and these samples decomposed gradually after 30 and 45 days. In contrast, the pure and metalloid samples could keep the initial smooth morphology without any change after long-time storage. Similar to the Sb case on the OIHP film and pure Sb film, the grains of Sb also appeared on the surface of the AIHP sample. To show the changes in these films more clearly, the photographs of all these samples were also taken and displayed in Figure 1e and Figure S7 (Supporting Information). For the OIHP film with Ag electrodes, the fresh film with silvery luster turned red after 25 days, which may be attributed to the reaction between the Ag and OIHP, such that AgI appeared in the sample. After 50 days, this film changed to yellow because the organic cations decomposed totally, and only the PbI<sub>2</sub> framework remained. For the OIHP film with Cu electrodes, the film's color also changed from its typical pinkish color to brown and at last came to yellow and dark red, where later we will prove that the yellow color was due to PbI<sub>2</sub> and dark red color came from the residual Cu. The AIHP films with Ag and Cu electrodes also apparently decayed, and the colors' changes were similar to the OIHP ones. In any case, all the metalloid samples showed metallic lusters after the 50-day storage, suggesting the perfect surfaces without any decay. These results indicate the exceptional stability of the metalloids acting as the electrodes of the halide perovskites.

To further investigate the decomposition mechanism of the OIHP with the metal electrodes and confirm the superior stability of the metalloid electrodes, XRD measurements were also performed on all these samples during the storage period. The corresponding XRD curves are illustrated in Figure 2a-c and Figures S8–S12 (Supporting Information). The XRD curves of the pure OIHP films shown in Figure S8 (Supporting Information) can maintain the same after the 50-day storage, revealing that the film did not decompose. It needs to be pointed out that apart from

the PbI<sub>2</sub> peaks located at 12.67° ((001) plane) and 38.66° ((003) plane), all the other peaks were from the quasi-2D OIHP film in Figure S8 (Supporting Information), which is commonly seen in the OIHP films.<sup>[36,37]</sup> All these peaks of the pure OIHP films could be found in the fresh samples with metal and metalloid electrodes. All the electrodes' peaks can also be detected except Si and Ge. It is because the Si and Ge films deposited by the thermal evaporation method are amorphous. However, for the Ag sample, there appeared the peaks of AgI located at 23.71° ((002) plane) and 39.20° ((110) plane) only after 10 days of storage, suggesting the iodide ions corroded the Ag electrodes in the OIHP film. As the storage time increased, the peak intensity of AgI and PbI<sub>2</sub> increased, and the intensity of the Ag and OIHP peaks decreased. After 20 days, the peaks from the Ag electrode disappeared, signifying that Ag was corroded totally and turned into AgI. For the Cu sample, the intensity of the PbI<sub>2</sub> peaks also increased as the storage time increased, indicating that the OIHP films decomposed gradually due to the Cu electrode. After 30 days of storage, the peaks of OIHP films located at 42.51° and 43.00° became weaker, and the peaks of CuI (220) plane located at 42.21° and Cu (111) plane located at 43.30° appeared, which confirmed Cu reacting with the OIHP film and turning into CuI. Gratifyingly, the XRD peaks of all the metalloid samples did not change a little after storage, suggesting the ultra-high stability of metalloids as electrodes for OIHPs. For the Au sample, there was also no obvious change in the XRD curves in Figure 2b after the 50 days of storage. Nevertheless, the intensity of the PbI<sub>2</sub> peak of the Au sample located at 12.67° increased slightly, showing the slight decomposition of OIHP films corresponding to the SEM images demonstrated above. In order to demonstrate the decay condition of these samples, the  $I_{\text{PbI}_2}/I_{\text{OIHP}}$  ratios were calculated and depicted in Figure 2d, where  $I_{\text{PbI}_2}$  and  $I_{\text{OIHP}}$  represent the peak intensities of the PbI<sub>2</sub> peak located at 12.67° ((001) plane) and the OIHP peak located at 14.06° ((111) plane) circled by blue dotted lines in Figures 2a-c. The  $I_{\text{PbI}_2}/I_{\text{OIHP}}$  ratios of Ag and Cu samples raised dramatically during storage because the electrodes reacted with the OIHP films violently. The  $I_{\text{PbI}_2}/I_{\text{OIHP}}$  ratio of the Au sample also increased gradually, contrasting with the metalloid and pure samples, which did not change after storage. These XRD results not only demonstrated the reaction process between the noble metals and the OIHP films but also strongly confirmed the unique chemical resistance of metalloids to halide perovskites.

For the evaluation of practical utilization, lateral-structured photodetectors were configured with the metal and metalloid electrodes, with a thickness of 50 nm, on the OIHP and AIHP films, where the schematic diagram of the device structure is shown in Figure S13 (Supporting Information). The metal and metalloid electrodes were thermally deposited on the perovskite film with the assistance of shadow masks, where the channel width and length were 70 and 10 μm, respectively. It is noted that because of the relatively low electrical conductivity of the pure Si film without doping, Ag film with a thickness of 50 nm was also deposited on the 20 nm thick Si film. The probe station equipped with a semiconductor analyzer was employed to measure the electrical properties of the devices, where the probes were used to electrically connect the semiconductor analyzer and the devices. The responsivities of OIHP and AIHP films based photodetectors with different electrodes are compiled in Table S2 (Supporting Information). Besides, the response speeds of

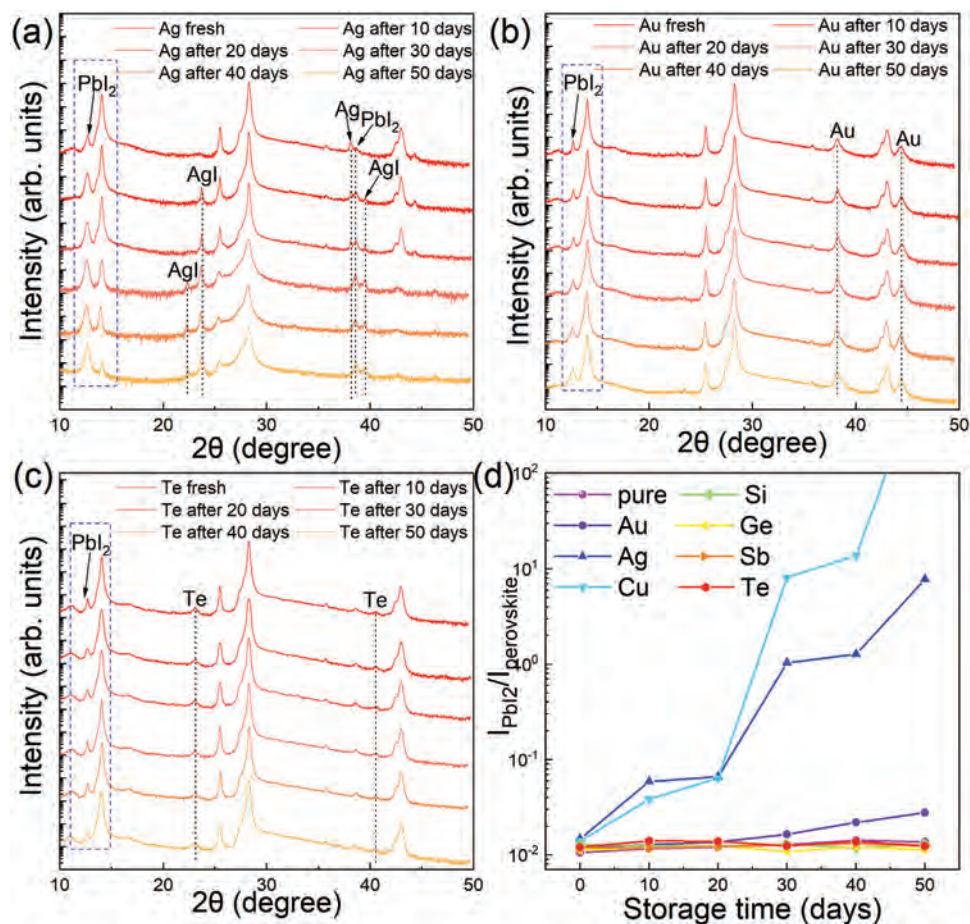


**Figure 2.** XRD curves of the OIHP films with a) Ag, b) Au, and c) Te electrodes during storage for 50 days. d) Changes in the  $I_{\text{Pbl}_2}/I_{\text{OIHP}}$  ratio of all the OIHP films with different electrodes during storage.

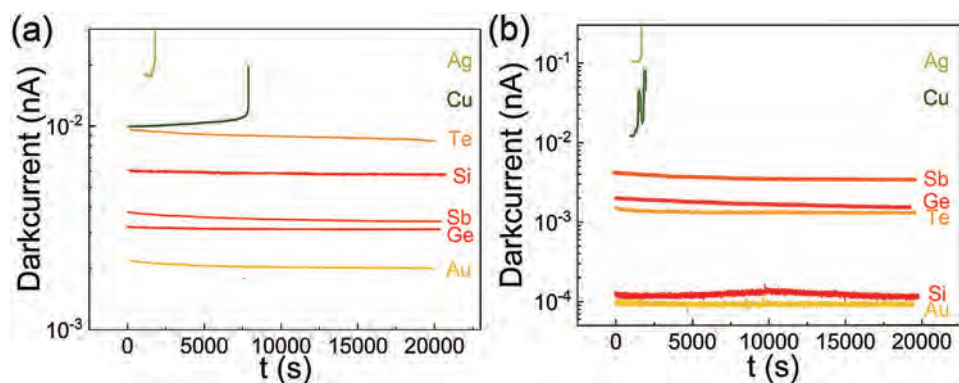


**Figure 3.** Long-time operation stability of the perovskite devices with different noble metal and metalloid electrodes based on a) OIHP and b) AIHP films.

these devices are also shown in Figures S14 and S15 (Supporting Information). One can see the device performance of the metalloid electrodes-based devices is comparable to or even better than the Au electrodes-based ones. In addition, the responsivity of the OIHP-based photodetector with Ge electrodes is a little lower than the others, which is caused by the relatively low work function of Ge. This result will as well be discussed later.

The long-time operation stability of the halide perovskites-based devices was then carefully studied. Specifically, a constant voltage of 1.5 V was applied to the devices in a dark box, where the channel width and length of the device were 70 and 10  $\mu\text{m}$ , respectively. As presented in **Figure 3a**, for the OIHP-based devices, Ag and Cu electrodes could only hold for hundreds of seconds. Then, the devices were short-circuited, causing the currents to

rise sharply because Ag and Cu had penetrated into the device channel during the operation. However, for Au and the metalloid electrodes, the devices could be in stable operation even after 20000 s. To assess the changes in the device performance after the long-time operation, one chopped laser with a wavelength of 450 nm and light intensity of 380 mW/cm<sup>2</sup> was applied to the devices before and after the operation. The on/off switching characteristics of the OIHP-based photodetectors are shown in Figure S16 (Supporting Information). After the extended operation, all metalloid samples could maintain their initial on/off characters. However, for the Au sample, the dark current of the device obviously increased, indicating the metastability of the Au electrode. It is worth mentioning that the on/off ratio of the Ge sample is lower than those of the other devices, which was caused by the low work function of Ge. The work functions of the metal and metalloid electrodes are listed in Table S1 (Supporting Information). Obviously, the work functions of all the metalloids are close to the conventional metal electrodes except Ge. However, the fermi levels of the different halide perovskites are different. For the perovskites with lower fermi levels, Ge and Sb can be chosen, and for those with higher fermi levels, Si and Te can be selected as the contact electrodes. Similarly, for AIHP devices, the long-time operation shown in Figure 3b also demonstrates that the metalloids and Au were much more stable than Ag and Cu as the electrodes of AIHP. Figure S17 (Supporting Information) shows the on-off switching current of the AIHP-based photodetector with a chopped laser. Evidently, the on/off ratio of the Au sample reduced after the operation, which again indicates that the Au electrode can also react with the perovskite material during the operation. More importantly, the long-time operation did not influence the metalloid samples, again proving their unique stability as electrodes. This evidence demonstrates that as the electrodes of halide perovskites, metalloids are far more stable than the conventional noble metals of Au, Ag, and Cu, which can perform much better in perovskite-based devices.

After that, first-principle calculations were performed to shed light on the stability and reaction mechanism of the metals and metalloids as electrodes for halide perovskites. From the XRD results, we know Ag and Cu can react with the OIHP film with the products of AgI, CuI, and PbI<sub>2</sub>. Accordingly, we can assume that if all the metals and metalloids would react with the OIHP film, the reaction equation would be:  $M + x\text{MAPbI}_3 = \text{MI}_x + x\text{MA} + x\text{PbI}_2$ , where M represents one kind of metal or metalloid and  $x$  is a coefficient of the reaction equation. For the metals and metalloids investigated in this work, the stable MI<sub>x</sub> is AuI, AgI, CuI, SiI<sub>4</sub>, GeI<sub>4</sub>, SbI<sub>3</sub>, or TeI<sub>4</sub>. All the free energies of the metals, metalloids, OIHP, and reaction products were calculated by the first-principles calculation method. The corresponding final reaction energies are presented in Figure 4a. One can see that the reaction energies of all the metalloids with OIHP are obviously larger than the conventional noble metals, indicating metalloids are harder to react with OIHP than the noble metals, agreeing well with the experimental results. Furthermore, we know that H<sub>2</sub>O can make the halide perovskites decompose quickly, which can even permeate the electrodes and react with the perovskites.<sup>[38]</sup> In this case, the absorption energies of the H<sub>2</sub>O molecule on metals and metalloids were calculated. We considered two possible absorption sites: on top of the metal or metalloid atom and the hollow site, where the typical structures were shown in Figure S18 (Sup-

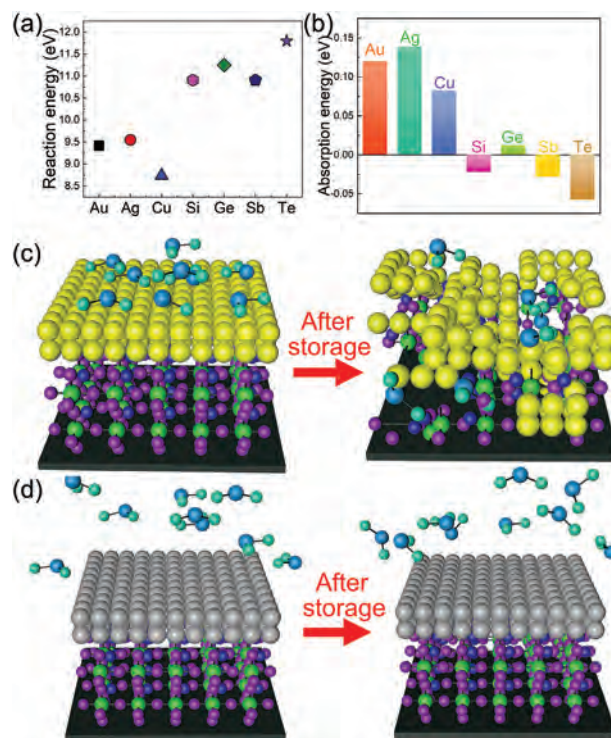


**Figure 4.** a) Reaction energies between the electrodes and the perovskite films. b) Absorption energies of H<sub>2</sub>O on different electrodes (H<sub>2</sub>O adsorbed on top of the metals or metalloids' atom). c) Schematic diagrams of the metal electrodes reacting with halide perovskites. d) Schematic diagrams of the metalloid electrodes protecting halide perovskites.

porting Information). For all the metals and metalloids, the absorption energies of the two absorption sites are revealed in Figures 4b and S19. In fact, the absorption energies of these two absorption sites are similar. The absorption energies of the noble metals are positive and much larger than those of the metalloids, suggesting H<sub>2</sub>O can easily be absorbed by these metals. Besides, the negative absorption energies of the metalloids of Si, Sb, and Te (only the absorption energy of Ge is positive, but it is also much smaller than those of the noble metals) indicate that these electrodes can even protect the perovskite films from being harmed by H<sub>2</sub>O. As demonstrated in Figure 4c, conventional noble metal electrodes can easily react with the halide perovskites, while the H<sub>2</sub>O they absorbed will also make the perovskites decompose violently. However, our metalloid electrodes in Figure 4d do not react with the halide perovskites. Not only that, but its ultra-high resistance to H<sub>2</sub>O can also protect the perovskite films from being broken down. The calculation further proves the superior stability of the metalloids over the noble metals as electrodes for halide perovskite and their exceptional resistance to H<sub>2</sub>O.

### 3. Conclusion

In conclusion, metalloid electrodes for halide perovskites were proposed and proved to be much more stable than the mostly used noble metal electrodes. The reaction mechanism between electrodes and perovskite films was also thoroughly studied through detailed characterization. More importantly, after being

configured to photodetectors, the excellent long-time operation stability of the metalloid electrodes was demonstrated in contrast to the relatively unstable noble metal electrodes. The first-principles calculations further confirm the unique stability of metalloids as the electrodes of halide perovskites. Besides, we found that H<sub>2</sub>O can hardly absorb onto the metalloids, which makes metalloids a protective layer for the underlying perovskite films. This work proposed one new kind of ultra-stable electrodes for halide perovskites, which can solve one of the main problems that impede the commercialization of halide perovskites-based electronic devices.

#### 4. Experimental Section

**Synthesis of Materials:** KI/I<sub>2</sub> solution was prepared by dissolving 400 mg of KI and 100 mg of I<sub>2</sub> in 4 ml of DI water. The OIHP precursor was prepared by dissolving iBA, MA, and PbI<sub>2</sub> at a molar ratio of 4:2:3 in dimethylformamide to form a 1 M solution. The AIHP precursor was prepared by dissolving CsBr and PbBr<sub>2</sub> at a molar ratio of 1:1 in dimethylsulfoxide to form a 0.5 M solution.

**Device Fabrication:** First, glass substrates were ultrasonically washed using acetone, ethanol, and deionized water for 15 mins in succession. These substrates were then treated with a mild oxygen plasma for 5 mins. For the OIHP films, 40 μL precursor solution was spin-coated on the glass substrate at 3000 rpm for 30 s, followed by thermal annealing at 100°C for 10 min. For the AIHP films, 40 μL precursor solution was spin-coated on the substrate at 3000 rpm for 30 s, followed by thermal annealing at 250°C for 10 min. After that, 50-nm-thick metal or metalloid electrodes were thermally evaporated onto the OIHP and AIHP films with the assistance of shadow masks to configure photodetectors, where the channel length and width are 10 and 70 μm, respectively.

**Film and Device Characterization:** The morphologies of the films were characterized using SEM (FEI Quanta 450 FEG SEM). The changes in the composition of the films were detected by XRD (D2 Phaser with Cu Kα radiation, Bruker). The thickness of the metal and metalloid films were confirmed by AFM (Dimension Icon, Bruker). The electrical performance of fabricated devices was characterized by a standard electrical probe station and an Agilent 4155C semiconductor analyzer (Agilent Technologies, California, USA). Lasers with a wavelength of 450 nm were used as the light sources for the photodetector measurement, while the power of the incident irradiation was measured using a power meter (PM400, Thorlabs). An attenuator was also employed to tune the irradiation power of the laser illuminating the device.

**Computational details:** The first-principles calculations were performed using density functional theory as implemented in the Vienna Ab initio Simulation Package.<sup>[39]</sup> The generalized-gradient approximation for exchange-correlation energy proposed by Perdew, Burke, and Ernzerhof was used.<sup>[40]</sup> The convergence criteria for the energy and atomic forces are set to 10<sup>-5</sup> eV and 0.01 eV Å<sup>-1</sup>, respectively. The Brillouin zone is sampled with G-centered 5 × 5 × 1 k point meshes.

#### Supporting Information

Supporting Information is available from the Wiley Online Library or from the author.

#### Acknowledgements

The authors acknowledge the General Research Fund (CityU 11306520) of the Research Grants Council of Hong Kong SAR, China, and the Foshan Innovative and Entrepreneurial Research Team Program (No. 2018IT100031).

#### Conflict of Interest

The authors declare no conflict of interest.

#### Data Availability Statement

The data that support the findings of this study are available from the corresponding author upon reasonable request.

#### Keywords

device degradation, electrode stability, halide perovskites, metalloids

Received: November 27, 2022

Revised: February 27, 2023

Published online: April 8, 2023

- [1] J. P. Correa-Baena, M. Saliba, T. Buonassisi, M. Grätzel, A. Abate, W. Tress, A. Hagfeldt, *Science* **2017**, 358, 739.
- [2] H. P. Wang, S. Li, X. Liu, Z. Shi, X. Fang, J. H. He, *Adv. Mater.* **2021**, 33, 2003309.
- [3] X. K. Liu, W. Xu, S. Bai, Y. Jin, J. Wang, R. H. Friend, F. Gao, *Nat. Mater.* **2021**, 20, 10.
- [4] A. K. Jena, A. Kulkarni, T. Miyasaka, *Chem. Rev.* **2019**, 119, 3036.
- [5] C. C. Boyd, R. Cheacharoen, T. Leijtens, M. D. McGehee, *Chem. Rev.* **2019**, 119, 3418.
- [6] B. Wook Park, S. Il Seok, *Adv. Mater.* **2019**, 31, 1805337.
- [7] N. Li, X. Niu, Q. Chen, H. Zhou, *Chem. Soc. Rev.* **2020**, 49, 8235.
- [8] A. R. Bin Mohd Yusoff, M. Vasilopoulou, D. G. Georgiadou, L. C. Palilis, A. Abate, M. K. Nazeeruddin, *Energy Environ. Sci.* **2021**, 14, 2906.
- [9] H. Yu, Y. Xie, J. Zhang, J. Duan, X. Chen, Y. Liang, K. Wang, L. Xu, *Adv. Sci.* **2021**, 8, 2004510.
- [10] C. H. Swartz, N. Khakurel, S. R. Najjar, M. I. Hossain, A. Zakhidov, *Phys. Status Solidi Appl. Mater. Sci.* **2021**, 218, 2000721.
- [11] S. Ma, Y. Bai, H. Wang, H. Zai, J. Wu, L. Li, S. Xiang, N. Liu, L. Liu, C. Zhu, G. Liu, X. Niu, H. Chen, H. Zhou, Y. Li, Q. Chen, *Adv. Energy Mater.* **2020**, 10, 1902472.
- [12] W. Lv, L. Li, M. Xu, J. Hong, X. Tang, L. Xu, Y. Wu, R. Zhu, R. Chen, W. Huang, *Adv. Mater.* **2019**, 31, 1900682.
- [13] L. Shi, M. P. Bucknall, T. L. Young, M. Zhang, L. Hu, J. Bing, D. S. Lee, J. Kim, T. Wu, N. Takamure, D. R. McKenzie, S. Huang, M. A. Green, A. W. Y. Ho-Baillie, *Science* **2020**, 368, 6497.
- [14] P. Pistor, A. Ruiz, A. Cabot, V. Izquierdo-roca, *Nat. Publ. Gr.* **2016**, 6, 35973.
- [15] N. N. Shlenskaya, N. A. Belich, M. Grätzel, E. A. Goodilin, A. B. Tarasov, *J. Mater. Chem. A* **2018**, 6, 1780.
- [16] C. Besleaga, L. E. Abramiuc, V. Stancu, A. G. Tomulescu, M. Sima, L. Trinca, N. Plugaru, L. Pintilie, G. A. Nemnes, M. Iliescu, H. Gud, A. Manolescu, I. Pintilie, *J. Phys. Chem. Lett.* **2016**, 7, 5168.
- [17] J. Li, Q. Dong, N. Li, L. Wang, *Adv. Energy Mater.* **2017**, 7, 1602922.
- [18] L. Zhao, R. A. Kerner, Z. Xiao, Y. L. Lin, K. M. Lee, B. P. Rand, *ACS Energy Lett.* **2016**, 1, 595.
- [19] S. Svanström, A. García-Fernández, T. J. Jacobsson, I. Bidermane, T. Leitner, T. Sloboda, G. J. Man, G. Boschloo, E. M. J. Johansson, H. Rensmo, U. B. Cappel, *ACS Mater. Au* **2022**, 2, 301.
- [20] S. Svanstro, T. J. Jacobsson, G. Boschloo, E. M. J. Johansson, H. Rensmo, U. B. Cappel, *ACS Appl. Mater. Interfaces* **2020**, 12, 7212.
- [21] Z. Hawash, L. K. Ono, Y. Qi, *Adv. Mater. Interfaces* **2018**, 5, 1700623.
- [22] D. Hao, J. Zou, J. Huang, *InfoMat* **2020**, 2, 139.
- [23] K. Domanski, N. Mine, M. K. Nazeeruddin, *ACS Nano* **2016**, 10, 6306.

- [24] W. Tress, M. Yavari, K. Domanski, P. Yadav, B. Niesen, J. P. Correa Baena, A. Hagfeldt, M. Graetzel, *Energy Environ. Sci.* **2018**, *11*, 151.
- [25] H. Han, U. Bach, Y. B. Cheng, R. A. Caruso, C. MacRae, *Appl. Phys. Lett.* **2009**, *94*, 2007.
- [26] C. Liu, M. Wu, Y. Wu, D. Wang, T. Zhang, *J. Power Sources* **2020**, *447*, 227389.
- [27] H. Zhang, K. Song, L. Zhu, Q. Meng, *Carbon N Y* **2020**, *168*, 372.
- [28] H. Wang, H. Liu, W. Li, L. Zhu, H. Chen, *Nano Energy* **2020**, *77*, 105160.
- [29] G. M. S. Alves, L. S. Rocha, H. M. V. M. Soares, *Talanta* **2017**, *175*, 53.
- [30] H. Li, K. Wang, H. Zhou, X. Guo, S. Cheng, K. Jiang, *Energy Storage Mater.* **2018**, *14*, 267.
- [31] S. Sun, M. Gao, G. Lei, H. Zou, J. Ma, C. Huang, *Nano Res.* **2016**, *9*, 1125.
- [32] S. M. Mercaptan, G. E. Fryxell, M. Gong, *Using*. No. September, **1997**.
- [33] D. H. Kim, H. C. Lee, *Jpn. J. Appl. Phys.* **1997**, *36*, L253.
- [34] C. Li, Z. Zang, C. Han, Z. Hu, X. Tang, J. Du, Y. Leng, K. Sun, *Nano Energy* **2017**, *40*, 195.
- [35] Z. Wang, F. Wang, W. Sun, R. Ni, S. Hu, J. Liu, B. Zhang, A. Alsaed, T. Hayat, Z. Tan, *Adv. Funct. Mater.* **2018**, *28*, 1804187.
- [36] S. Shahbazi, C.-M. Tsai, S. r Narra, C.-Y. Wang, H.-S. Shiu, S. Afshar, N. Taghavinia, E. W.-G. Diau, *J. Phys. Chem. C* **2017**, *121*, 3673.
- [37] J. Chen, J. Xu, L. Xiao, B. Zhang, S. Dai, J. Yao, *ACS Appl. Mater. Interfaces* **2017**, *9*, 2449.
- [38] Y. Kato, L. K. Ono, M. V. Lee, S. Wang, S. R. Raga, Y. Qi, *Adv. Mater.* **2015**, *2*, 1500195.
- [39] G. Kresse, J. Furthmüller, *Phys Rev B Condens Matter Mater Phys* **1996**, *54*, 11169.
- [40] J. P. Perdew, K. Burke, M. Ernzerhof, *Phys. Rev. Lett.* **1996**, *77*, 3865.